ON THE ROLE OF IRON OXIDES IN THE ELECTROCHEMICAL BEHAVIOUR OF STEEL EMBEDDED IN CONCRETE

X.R. Nóvoa* and M.C. Pérez

University of Vigo, E.T.S.E.I., Lagoas-Marcosende, 9,

36200 Vigo, Spain

ABSTRACT

Magnetite is a common product of iron corrosion and oxidation processes. This mixed Fe^{2+}/Fe^{3+} oxide can transform reversibly into species having higher or lower oxidation degree than the stoichiometric 1:2 Fe^{2+} to Fe^{3+} ratio. The redox activity associated to magnetite transformations is of major importance in alkaline solutions as those found in concrete pores solution and can mask the electrochemical response corresponding to iron corrosion. The present paper discusses the state of the art on this aspect. It appears that the electrode potential (or the corrosion potential) is a key parameter necessary for assessing steel rebars corrosion rate as well as for defining the critical ratio Cl^- to OH^- necessary for rebar depassivation.

1. INTRODUCTION

Almost half a century ago the original papers by Stern[1,2,3] demonstrated the relationship between corrosion current density, i_{corr}, and the slope of the steady state polarisation curve, named Polarisation Resistance, Rp. Since that time the formula given in equation 1 (the Stern-Geary equation[4]) has come into general use to obtain kinetic information about corrosion processes.

$$i_{corr} = B/Rp \qquad (1)$$

* Corresponding author. Tel.: +986812213, Fax.: +986812201, E-mail: rnovoa@uvigo.es

As the conditions highlighted by Stern (the corrosion potential shall be far enough from the reversible potentials of the anodic and cathodic reactions, charge transfer shall be the controlling process, no significant ohmic drop is present, etc) are rarely fulfilled, equation 1 is usually employed in a qualitative way or in a quantitative one after calibration with weight loss determinations for each particular application, using the constant B as "fitting" parameter. Values of B between 10 and 45 mV have been found for low alloy steels in acid and alkaline environments[1], and so the commonly employed value for B, 26 mV, guarantees that the corrosion rate estimation approaches the true corrosion rate by about ±50%.

Since the late 80's the corrosion rate of steel rebars in concrete is commonly measured using the polarisation resistance method, once weight loss determinations allowed defining the experimental conditions (potential sweep rate and B values) for good agreement with electrochemical measurements[6] using equation 1. Moreover, throughout the 90's different electrochemical methods have also been used for this purpose[7]. Potentiostatic and galvanostatic pulses[8, 9] Electrochemical Impedance Spectroscopy (EIS)[10] and Cyclic Voltammetry[11, 12], can be cited among the techniques able to give the Rp parameter. The introduction of different techniques has evidenced difficulties in obtaining concordant results, difficulties that can be overcome if the redox activity of the corrosion products is considered[13]. This aspect is the central subject of the present review.

Concrete is an intrinsically porous material. The electrolyte in the concrete pores constitutes the ionic path for the electrical signals to reach the reinforcing bars; so, the electrical properties of the concrete cover (which can be analysed to get structural information[14, 15, 16]) can mask the rebar's electrochemical response, as it happens for example with corrosion potential readings. Potential mapping is the most commonly used electrochemical technique to assess the rebar's corrosion[17] on real structures. Nevertheless, some doubts have arisen about the real meaning of the measured electrode potentials due to the many different phenomena present in the concrete bulk that can influence the measured potential. Diffusion potentials, membrane potentials and streaming potentials can be cited among such factors[18]. The procedure described in ASTM C876 standard[19] for pre-wetting concrete surfaces tends to minimize those effects.

Potential mapping gives only qualitative information. If quantitative data have to be obtained then it is necessary to polarise the steel rebar in some way (dc. or ac. techniques). The only exception is Electrochemical Noise

Analysis, ENA, which is a non-perturbing technique that, according to some authors[20], allows obtaining kinetic information, although considerable uncertainties remain when the technique is applied to steel in concrete[21]. As the electrochemical parameter needed to obtain the rebar corrosion rate is the corrosion current density, i_{corr}, the objective of the various electrochemical methods mentioned above is the determination of the polarisation resistance, because this is related to corrosion rate through equation 1, if Rp is obtained free of cover-concrete contributions (i.e. corrected for ohmic drop) and the system fulfils the conditions highlighted by Stern (mentioned above).

The discussion in the present review is focused in the electrochemical behaviour at the rebar-concrete interface, disregarding the dielectric contribu tion of the concrete cover that, in the frequency range of interest, will represent just a "series resistance" or "electrolyte resistance" responsible of the ohmic drop.

2. ELECTROCHEMISTRY OF IRON IN ALKALINE MEDIA.

The electrolyte in concrete pores is strongly alkaline[22], and its pH can be as high as 13. So, for corrosion investigations on this electrochemical system, it is important to know the anodic behaviour of iron in a strongly alkaline medium. Such a study was largely carried out in the 70's as a candidate of a battery electrode[23-30]; nevertheless, the dissolution and passivation mechanisms still remained unclear.

Recently, additional effort has been focused in understanding the electrochemical properties of the oxides layer developing on iron in alkaline media[31-33]. Different electrochemical techniques have been employed for this purpose: Cyclic Voltammetry, Electrochemical Impedance Spectroscopy (EIS), Electrochemical Quartz Crystal Microbalance (EQCM), *in situ* Raman Spectroscopy, and Rotating Ring-Disk Electrode (RRDE).

Stationary iron electrodes polarised in low scan rate Cyclic Voltammetry tests[31] show six oxidation peaks in the forward (anodic) sweep and five reduction peaks in the reverse (cathodic) sweep, as can be seen in Figure 1.

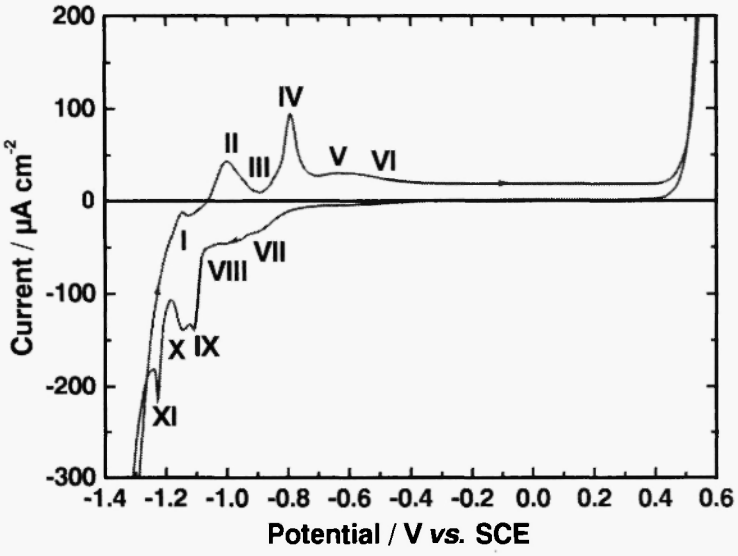

Fig. 1: Voltammogram of stationary Fe electrode. dE/dt = 0.5 mV s^{-1} in NaOH 1M. Current peaks are marked I to XI. (From reference 33)

The peaks III, V, VI for the anodic and VII for the cathodic sweep are only observed for stationary electrodes and also for an extremely low potential sweep rate, as used in the cited literature[31,33]. The texture of surface film therefore plays a determining role to the appearance of those peaks. Peak assignation is as follows[32]:

The peaks II, III for anodic and X, XI for cathodic sweep are attributed to the reaction given in equation 2:

$$Fe^0 + 2OH^- \rightleftharpoons Fe(OH)_2 + 2\,e^- \qquad (2)$$

The peak III is related to the oxidation of Fe^0 formed by the disproportionation reaction in the surface film (equation 3):

$$4\,Fe(OH)_2 \rightleftharpoons Fe^0 + Fe_3O_4 + 4\,H_2O \qquad (3)$$

The peaks IV and IX are due to the formation of magnetite according to equation 4:

$$3\ Fe(OH)_2 + 2\ OH^- \rightleftharpoons Fe_3O_4 + 4\ H_2O + 2\ e^- \quad (4)$$

Beyond the peak IV, magnetite partially oxidises to γ-FeOOH according to equation 5, to which peaks V, VI, VII and VIII correspond.

$$Fe_3O_4 + OH^- + H_2O \rightleftharpoons 3\ FeOOH + e^- \quad (5)$$

The splitting into two peaks suggests the presence of two surface layers and each peak corresponds to the oxidation of Fe_3O_4 to FeOOH at outer and inner layer. FeOOH will be then transformed chemically into Fe_2O_3 in a dehydration process (equation 6).

$$2\ FeOOH \rightleftharpoons Fe_2O_3 + H_2O \quad (6)$$

In situ Raman spectroscopy indicates[33] the presence of magnetite all over the interval of potentials depicted in Figure 1, so the redox processes corresponding to equations 4 and 5 should be considered when discussing iron corrosion rate, which actually corresponds only to the forward reaction in equation 2. Moreover, RRDE experiments show that beyond peak IV the outermost part of the passive film is composed mainly of Fe^{+3} species, while Fe^{+2} appears at electrode potential values lower than that corresponding to this peak, as can be deduced from the ring current depicted in Figure 2. So, the magnetite-based passive film seems to present a layered structure with increasing Fe^{+3}/Fe^{+2} ratio from the iron substrate towards the solution interface, concentration profile that is electrode potential dependent. Such type of structure was found also by *ex situ* techniques[34].

EQCM allows direct information to be obtained about mass changes occurring at the metal-oxide system. Figure 3 shows that, for potential values lower than –0.7 V, the passive film incorporates electrolyte (reverse equation 4), breaks down and partially leaves the electrode. This figure also shows that the overall electrode mass decreases from cycle 1 to 3 (i.e., see mass values at + 0.4V). This mass loss on time corresponds to the iron corrosion rate. Nevertheless, the feature of each cycle at electrode potentials more noble than –0.7V is different in the forward and reverse directions (increasing and decreasing potential, respectively). For the reverse direction, the curve is almost a horizontal line, i.e., no net mass loss is measured. So, a parallel process (which has been attributed[33] to electrolyte ingress into the oxide

film) compensates the mass loss due to corrosion. This process corresponds to equation 6.

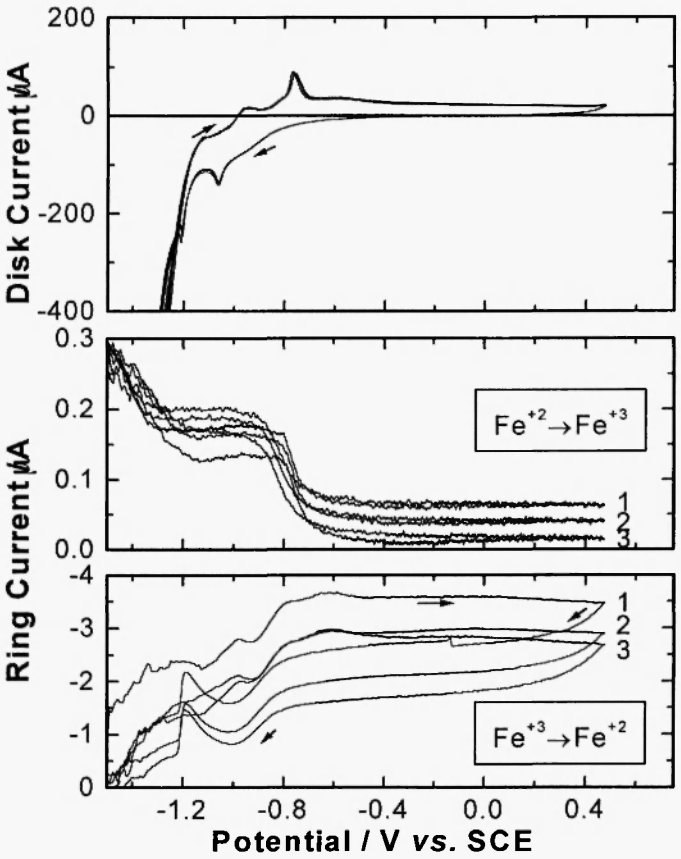

Fig. 2: RRDE experiments. Iron disk (5 ϕ mm) and glassy carbon ring (5.1 ϕ mm, $''_{in}$, 7 ϕ mm, $''_{ext}$). Collection efficiency N_0= 0.463. dE_{disk}/dt = 1mV s^{-1}. The labels in the figure correspond respectively to the 1st, 2nd and 3rd cycles of disk potential sweep. The ring potential for collection of Fe^{3+} was –1.13. V, and that for Fe^{2+} was +0.125 V vs SCE. (From reference 33)

The passive film hydration degree is a very important parameter in corrosion behaviour. As classical textbooks[33] refer, the surface charge

depends on this parameter. So, a surface charged negatively will hinder chloride adsorption making the system resistant to pitting. Such approach allows explaining recent results[36] that show a dependence of the pitting potential of steel embedded in concrete on the electrode potential and the $[Cl^-]/[OH^-]$ ratio necessary for steel depassivation. This ratio increases with electrode potential up to about +0.4V vs. SCE where the rebars are resistant to pitting. According to the given EQCM data, a passive film resistant to Cl^- corresponds to a highly dehydrated situation. The old controversy concerning the maximum $[Cl^-]/[OH^-]$ ratio acceptable to avoid rebar corrosion[37] seems to be over because it is meaningless without reference to the rebar's corrosion potential, which determines the hydration degree in a passive situation.

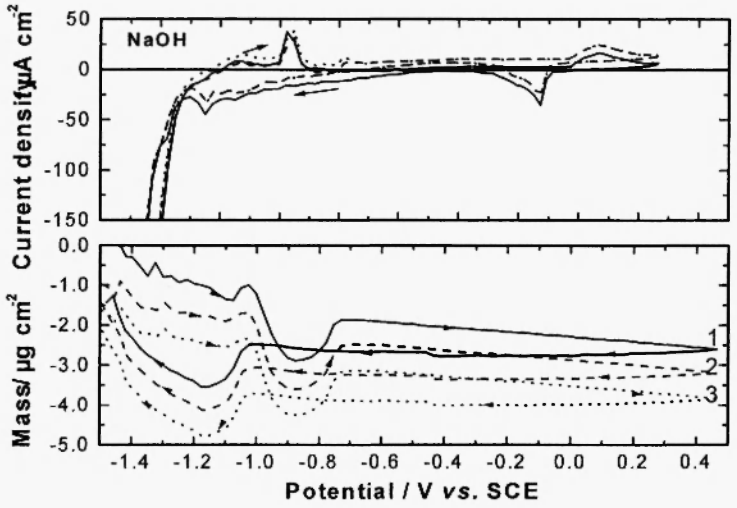

Fig. 3: Quartz crystal microbalance measurements on stationary electrode of electrodeposited Fe (5 ϕ "mm) in 1M NaOH. Potential sweep rate = 1mV s^{-1}. The labels in the figure correspond respectively to the 1st, 2nd and 3rd cycles of electrode potential sweep. (From reference 33).

The presence of several redox processes developing simultaneously at the metal-electrolyte interface is also evident from EIS measurements. Besides chloride containing media where three time constants were observed in the impedance spectra[32, 33], EIS plots show typically the shape depicted in Figure 4 where two time constants are present: at about 100 and 0.1 Hz.

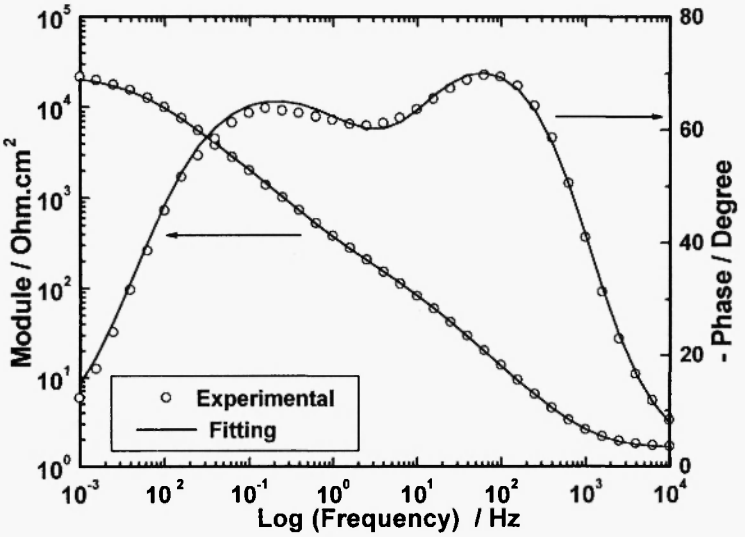

Fig. 4: Left, impedance spectrum (dots) obtained for the stationary Fe electrode in 1M NaOH at E= –0.45 V. Experimental results were fitted using two hierarchically distributed RC time constants (equivalent circuit and corresponding equation for Z(ω) on the right). The best-fitting parameters giving the solid line representation on the left are:[33]

R_0 /Ω.cm^2	R_1 /Ω.cm^2	C_1/μF.cm^{-2}	α_1	R_2/kΩ.cm^2	C_2/mF.cm^{-2}	α_2
1.6	236	179	0.8779	23.4	1.03	0.7425

Considering the high frequency time constant (R_1C_1 in Figure 4) associated to the double layer capacitance in parallel with the charge transfer resistance, and the low frequency time constant (R_2C_2 in Figure 4) associated to an additional redox process, the experimental data can be modelled all over the potential range. The relevant aspect here corresponds to the dependence of C_1 and C_2 on the electrode potential. This dependence is summarised in Figure 5. C_2 values are always higher than C_1 values and both profiles roughly follow the voltammogram depicted in Figure 1.

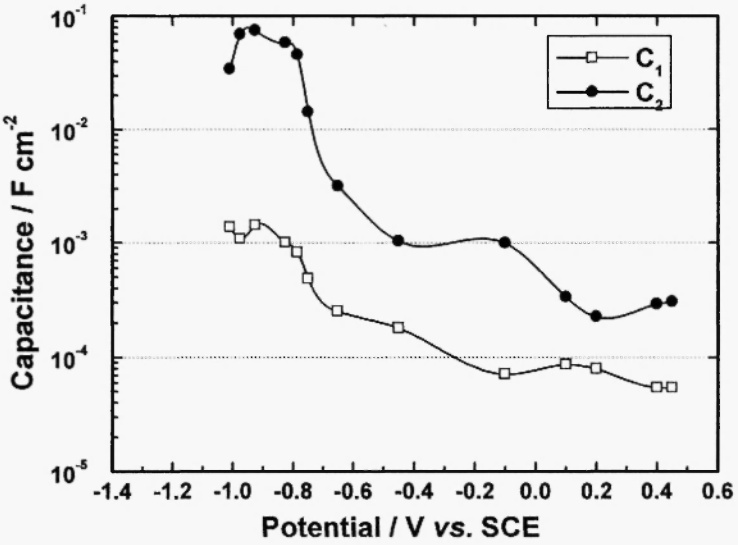

Fig. 5: Electrode potential dependence of capacitances C_1 and C_2. These values were obtained by fitting experimental impedance data (from the stationary Fe electrode in 1M NaOH) to the equivalent circuit depicted in Figure 4.

For potential values more noble than about –0.4V, C_1 become lower than 100 $\mu F.cm^{-2}$, values that can be considered as typical for double layer capacitance[38]. So, only in this potential range the assumption of double layer capacitance-charge transfer resistance can be assumed. And also in this potential range the C_2 values can be attributed to the redox process depicted in equation 5 because –0.4V is beyond peak VI, which according to Figure 1, is the last one appearing in the anodic sweep.

It is perhaps interesting to recapitulate here that the redox capacitance (also called pseudo-capacitance) corresponds to equation 7, where q_t represents the total amount of charge stocked (about 1 mC per monolayer), and 0 is the unit fraction of charge transformed at the potential value E. The maximum of C_{redox} is then reached for $\theta = 0.5$, where $d\theta/dE$ has its maximum. For lower and higher potential values $d\theta/dE$ decreases exponentially. A detailed analysis on this aspect can be found in the literature[39-41].

$$C_{redox} = q_t \frac{d\theta}{dE} \quad (7)$$

Thus, beyond peak VI only the redox process given in equation 5 will contribute significantly to C_{redox} (C_2 in Figure 5) whose value decreases as the electrode potential goes anodically because $d\theta/dE$ decreases. For electrode potentials lower than –0.4V the redox processes given in equations 5, 4 and 2 (this in the far cathodic region) are dominant in both time constants and the corresponding capacitances increase consequently. So, an accurate estimation of iron corrosion (equation 2) will only be possible from the high frequency time constant, for electrode potential values higher than that corresponding to peak VI.

3. ELECTROCHEMISTRY OF STEEL REBARS IN CONCRETE.

3.1. Cyclic Voltammetry studies.

The thickness of the oxides layer, which can reach 5 μm for rebars embedded in concrete after three years of atmospheric exposure, and the degree of crystallinity and compactness reached make a great difference between passive layers formed in solution (referred to above) and those formed in natural conditions. Nevertheless, the voltammograms shown in Figures 1 and 6 are still comparable[42]. Besides the difference in potential scales (which can be attributed to the referred difference in crystalline states), both voltammograms show active-passive behaviour in which the activity peak (at about –0.3V in Figure 6) corresponds to peak IV in Figure 1. So, according to the discussion in previous section, the electrochemical behaviour of passive steel in concrete will be highly influenced by the redox processes given in equations 2, 4 and 5.

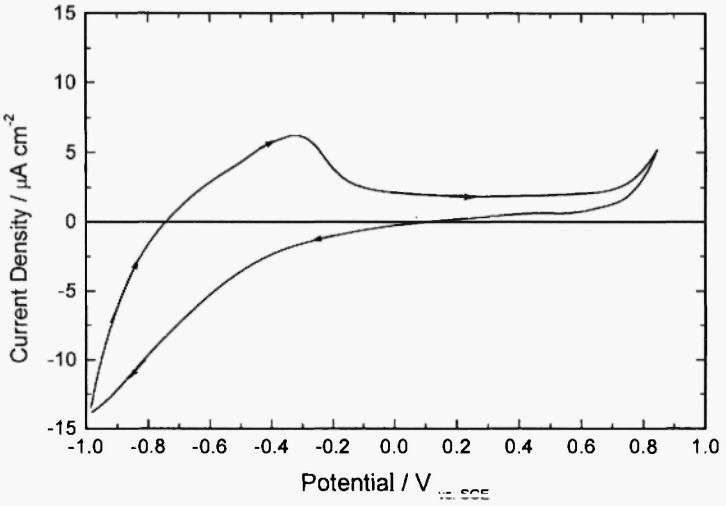

Fig. 6: Voltammogram obtained at 0.5 $mV.s^{-1}$ for a steel rebar embedded in concrete, after 3 years ageing in the atmosphere (from ref. 42).

3.2. EIS studies.

Electrochemical Impedance Spectroscopy has been applied to study corrosion of steel in concrete since the early eighties[43]. Two regions can be differentiated in the impedance spectra: the high frequency region (frequency higher than about 100 Hz), that originally was attributed to some inorganic layer formed on the steel surface[43], and more recently to the concrete cover contribution[44]; and the low frequency region, which corresponds to the electrochemical reactions developing at the steel-concrete interface. The high frequency part of the spectra is highly dependent on the electrode arrangement[45], but this aspect will not be discussed here further because it is outside the scope of the present review.

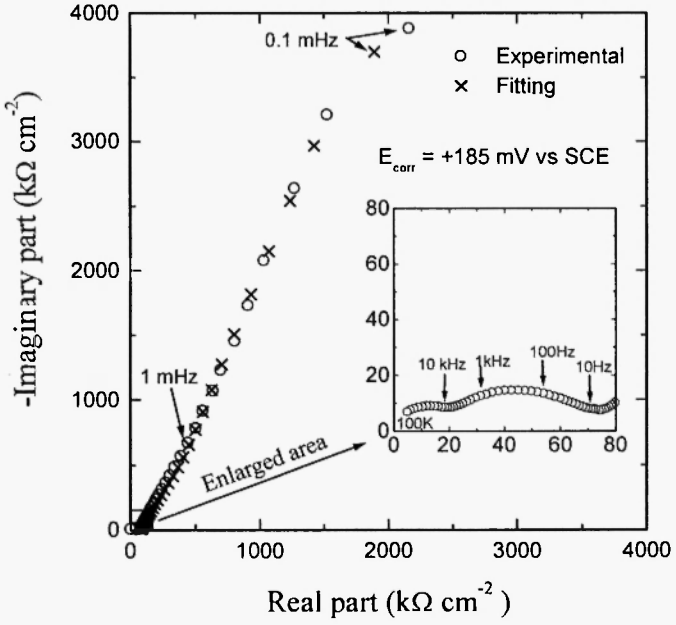

(a)

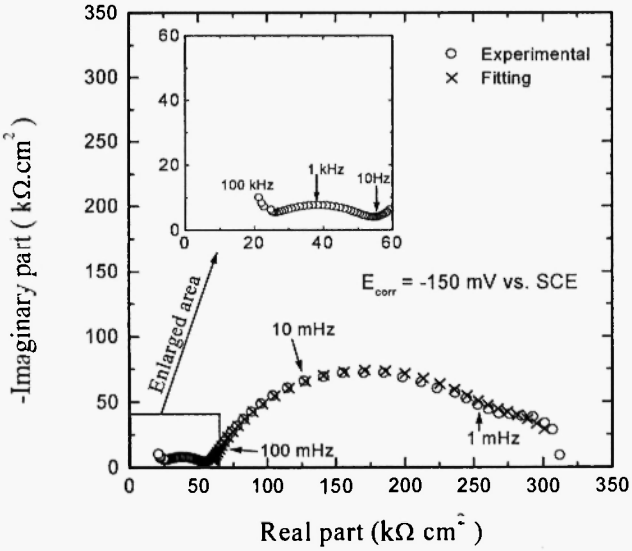

(b)

Fig. 7: (from ref. 48). Complex plane impedance plots obtained on an eight year atmosphere-aged probe in dry conditions at E_{corr} = +185 mV (a)

and after one day wetting at E_{corr} = -150 mV (b). Dots correspond to the experimental data and crosses to the fitting using the equivalent circuit depicted in figure 4. The best fitting parameters are:

Data	R_0(kΩ cm^2)	R_1(kΩ cm^2)	C_1(μF cm^{-2})	α_1	R_2(Ω cm^2)	C_2(mF cm^{-2})	α_2
(a)	83.0	464	101	0.788	$2x10^9$	2.9	0.673
(b)	57.6	230	112	0.730	$31.5x10^3$	15.5	1.0

The impedance spectra in the low frequency range (f< 10-100 Hz) show typically two time constants, and some Nyquist diagrams present constant phase lines in the very low frequency range, which has led to the widely accepted interpretation of double layer capacitance in parallel with corrosion resistance plus diffusion (Warburg) impedance[46, 47]. In Figure 7(a) this kind of diffusion behaviour can be observed for a dry specimen; nevertheless, if the same probe is sprayed with water, the impedance spectra shown in Figure 7(b) are obtained. Recently[48] an interpretation has been advanced for such behaviour. The corrosion potential shifts cathodically from dry to wet situations (which is coherent with oxygen availability at the steel-concrete interface) but it remains anodic to the magnetite formation peak (about –0.3 V vs. SCE according to Figure 6). In that condition the reactions given in equations 2 and 4 are irreversible and will be coupled to the double layer capacitance, while magnetite oxidation/reduction (equation 5) is reversible in this potential range and so will appear in the impedance spectra as a time constant having a capacitance proportional to the amount of active matter (represented in equation 7 by q_t). The arc in Figure 7 having a characteristic frequency close to 10 mHz will correspond to the charge transfer for iron dissolution in parallel to the double layer capacitance, while it is at frequencies lower than 1 mHz when magnetite redox response appears. The associated capacitance changes very much from dry to wet conditions (see C_2 fitting values in the Figure caption) due probably to electric conductivity changes in the oxide layer. This capacitance change is responsible for the dramatic modification observed in the impedance spectra from dry to wet conditions.

3.3. Macro-galvanic coupling.

The reversibility of Fe_3O_4 oxidation to γ-Fe_2O_3 has already been established in the early eighties[49]. Based upon this property and taking into account that Fe_3O_4 and γ-Fe_2O_3 form the passive layer on iron in alkaline

media[50], one decade later it was possible to postulate this redox process as responsible for the time constant appearing in the micro-hertz range of the impedance spectra[40, 44]. This time constant has been attributed to diffusion phenomena by various authors[46,47]. The existence of a redox couple in the rebar-concrete interface allows interpreting the changes observed in galvanic coupling current[51, 52].

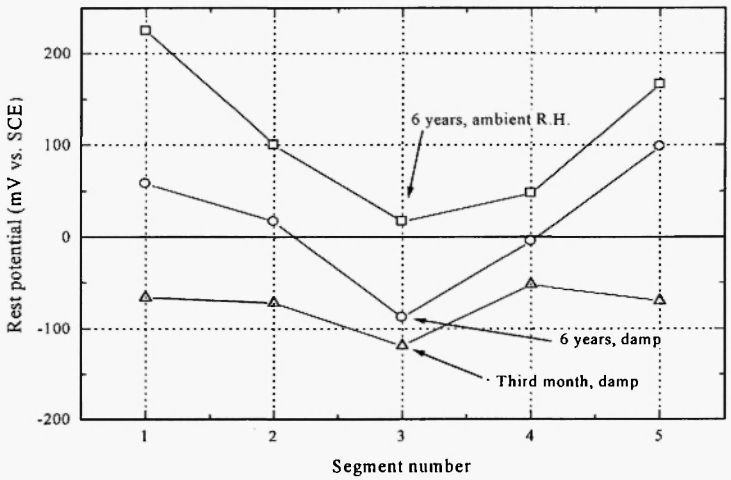

Fig. 8: Change of the corrosion potential of the individual rebar segments of a segmented concrete beam (1 m length) with ageing and degree of wetness. Segment N÷ 3 contains 3%$CaC\ell_2$ to induce active corrosion. (From reference 52).

Figure 8 shows that the corrosion potential is highly dependent on ageing and degree of wetness. Anhydrous corrosion products permit the flow of electrons from the anodic sites to reduce Fe^{3+} species (reverse equation 5). This additional cathodic reaction shifts the corrosion potential in the noble direction (as shown also in Figure 7). Thus, the ageing of corrosion products can be regarded as chemical oxidation of Fe^{2+} species while drying is involved in electrochemical reduction of Fe^{3+} species previously formed.

Figure 8 shows that, for example, segment 2 in wet condition has almost the same potential as segment 3 in dry. So, the macro-galvanic action is quite limited in heterogeneous structures. Moreover, the over-production of

corrosion products in the macrocell anodic sites leads to a kind of active passivation resulting in a cathodic behaviour for these sites when the concrete reduces its R.H. to a certain value. Thus, a final state will be reached in which the activity between anodic and cathodic sites results balanced, reducing or eliminating macro-cell activity. It has been demonstrated[53] that macro-cell effects are limited to a close neighbourhood of anodic sites (the cathodic surface being about ten times the anodic one), representing the galvanic current a maximum of 53% of the corrosion rate due to micro-cell activity.

3.4. Corrosion rate assessment.

The meaning of R_I and C_I parameters is clear for Figure 7; nevertheless, the situation is not so clear when the corrosion potential shifts cathodically towards the magnetite formation peak. At about –0.3 V vs. SCE the magnetite formation peak (equation 4) is observed in Figure 6. At even more cathodic potential values, the system approaches the cathodic protection domain where the Fe/Fe^{2+} redox process (equation 2) is also present. Under those circumstances R_I cannot be considered anymore as associated to iron corrosion but to the corresponding redox process rate. The conditions highlighted by Stern[1-4] for equation 1 being applicable are not fulfilled. The R_I data depicted in Figure 9 illustrate this aspect: only in the potential range –0.2 to +0.5 V R_I values are compatible with the existing passive situation and correspond to the charge transfer resistance for iron corrosion (so identifiable with R_p). Out of this potential range R_I values decrease due to the presence of parasite processes and do not measure iron corrosion.

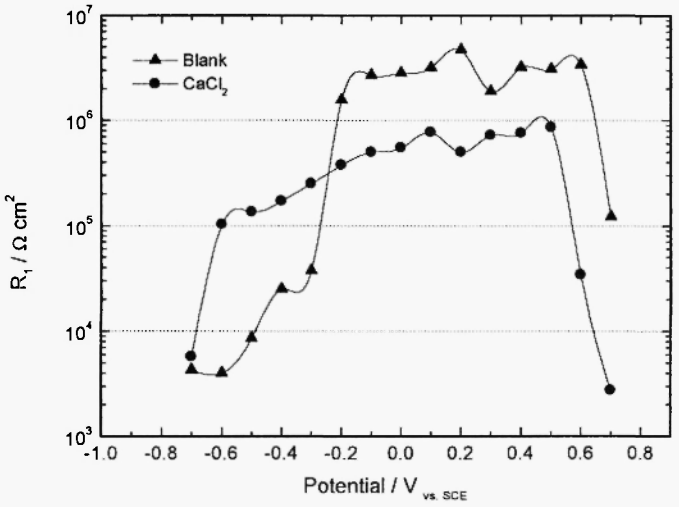

Fig. 9: Dependence of the resistance, R_1, on the electrode potential at three years of ageing for a rebar embedded in plain concrete (triangles) and in concrete with 2% $CaCl_2$ added (from ref. 42).

In Figure 10 the optimal conditions empirically established by Andrade *et al.*[6] for R_p determination are given. The selected polarisation rate range (2 to 10 $mV.min^{-1}$) represents a frequency range from 0.8 to 8 mHz (a detailed analysis of equivalences between scan rate, waiting time and frequency can be found in a recent paper[54] paper by Scully). The physical basis for measuring R_p not at the steady state, but to a certain sweep rate/waiting time has been advanced recently[48]: The real part of the impedance at 1 mHz closely corresponds (see Figure 7) to $R_1 + R_0$; so, once correction for IR drop (R_0), the measured resistance at this frequency can be taken as the charge transfer for iron corrosion. As can be seen also in Figure 7 the impedance close to 1 mHz is highly dependent on frequency for dry condition while its variation on frequency is lower for wetted specimens. This is the reason why most practices recommend pre-wetting the structure prior R_p measurements.

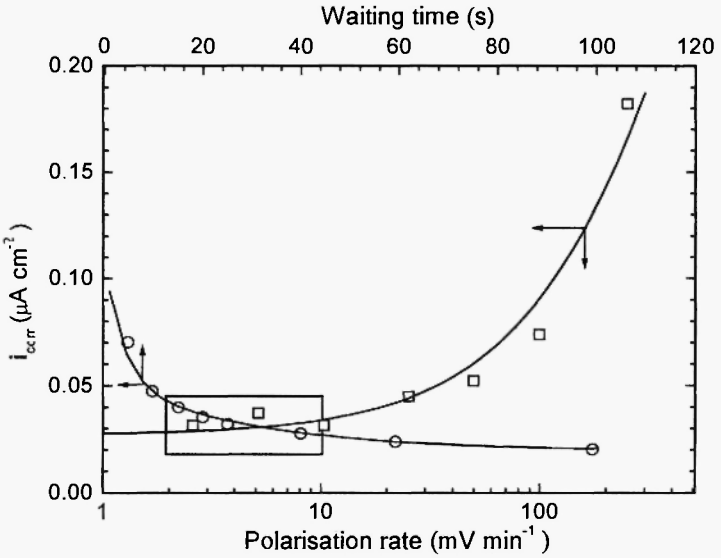

Fig. 10: Polarisation rate (or waiting time after potentiostatic step) vs. corrosion rate of steel in concrete. The inserted rectangle delimits the optimal conditions to get good correlation between electrochemical and gravimetric data. (Adapted from ref. 6).

4. CONCLUSIONS

The reviewed literature shows that the electrochemical response of steel in concrete is determined to a great extent by magnetite redox activity. In the potential range above the magnetite formation peak (centred at about –0.3 V vs. SCE) it is possible to obtain R_p values associated to steel corrosion, while for potential values cathodic to –0.3 V the relative importance of the Fe^{2+}/Fe reduction reaction increases as the potential proceeds in the cathodic direction. Under those circumstances the obtained R_p values do not correlate directly with the rebar's corrosion rate.

Moreover, as the electrode potential moves in the noble direction, the oxides layer dehydrates, which increases the layer's resistance to passivity breakdown by the presence of chlorides.

REFERENCES

1. M. Stern, R.M. Roth, *J. Electrochem. Soc.* **104**, 390 (1957).
2. M. Stern, *Corrosion-NACE*, **13**, 775t (1957).
3. M. Stern, *Corrosion-NACE*, **14**, 329t (1958).
4. M. Stern, A.L. Geary, *J. Electrochem. Soc.* **104**, 56 (1957).
5. L.M. Callow, J.A. Richardson, J.L. Dawson, *Br. Corros. J.* **11**, 123 (1976).
6. C. Andrade, V. Castelo, C. Alonso, J. A. Gonzalez, in: *Corrosion Effect of Stray Currents and the Techniques for Evaluating Corrosion of Rebars in Concrete.* V. Chaker (Editor), p 43. ASTM STP 906, American Society for Testing and Materials, Philadelphia, 1986.
7. B. Elsener, *Mater. Sci. Forum*, **192-194**, 857 (1995).
8. G.K. Glass, C.L. Page, N.R. Short, J.-Z. Zhang. *Corros. Sci.* **39**, 1657 (1997).
9. K. Videm, *Mater. Sci. Forum*, **289-292**, 3 (1998).
10. L. Hachani, C. Fiaud, E. Triki, A. Raharinaivo, *Br. Corros. J.*, **29**, 122 (1994).
11. J.T. Hinatsu, W.F. Graydon, R. R. Foulkes, *J. Appl. Electrochem.* **21**, 425 (1991).
12. J. Flis, H.W. Pickering, K. Osseo-Asare, *Electrochim. Acta,* **43**, 1921 (1998).
13. K. Videm, *Electrochim. Acta,* **46**, 3895 (2001).
14. M. Keddam, H. Takenouti; X. R. Nóvoa, C. Andrade, C. Alonso, *Cem. Conc. Res.* **27**, 1191 (1997).
15. C. Andrade, V. M. Blanco, A. Collazo, M. Keddam, X. R. Nóvoa, H. Takenouti, *Electrochim. Acta*, **44**, 4313 (1999).
16. M. Cabeza, P. Merino, A. Miranda, X.R. Nóvoa, I. Sanchez, *Cem. Conc. Res.* **32**, 881 (2002).
17. K. Videm, in: *Corrosion of Reinforcement in Concrete, Monitoring, Prevention and Rehabilitation*, J. Mietz, B. Elsener and R. Polder (Eds.), p 104. Publication No 25 in European Federation of Corrosion Series published by The Institute of Materials, London, 1998.
18. H. Arup, O. Klinghoffer, in: *Corrosion of Reinforcement in Concrete, Monitoring, Prevention and Rehabilitation*, J. Mietz, B. Elsener and R. Polder eds. p 31. Publication No 25 in European Federation of Corrosion Series, published by The Institute of Materials, London, 1998.

19. *ASTM Annual Book of ASTM Standards*. Volume 03.02. Wear and Erosion, Metal Corrosion. p.11. ASTM, West Conshohocken, PA, USA, 1998.
20. F. Mansfeld, H. Xiao, *J. Electrochem. Soc.*, **140**, 2205 (1993).
21. U. Bertocci, in: *Electrochemical Noise Measurement for Corrosion Applications*, ASTM STP1277, J. R. Kearns, J. R. Scully, P. R. Roberge, D. L. Reichert and J. L. Dawson (Eds.), p.39. ASTM, West Conshohocken, PA, USA, 1996.
22. H.F.W. Taylor, *Cement Chemistry* (2nd Edn), p. 214, T. Telford Pub, London, 1998.
23. D. M. Drazic, C. S. Hao, *Electrochim. Acta,* **27**, 1409 (1982).
24. C. Chanson, P. Blanchard, *J. Electrochem. Soc.* **136**, 2862 (1989).
25. D. D. MacDonald, B. Roberts, *Electrochim. Acta,* **23**, 781 (1978).
26. T. Zakroczymski, Fan Chweir-Jer, Z. Szklarska-Smialowska, *J. Electrochem. Soc.* **132**, 2862 (1985).
27. T. Zakroczymski, Fan Chweir-Jer, Z. Szklarska-Smialowska. *J. Electrochem. Soc.* **132**, 2868 (1985).
28. S. Haupt, H.-H. Streblow, *Lagmuir*. **3**, 873 (1987).
29. S. Juanto, J.O. Zerbino, M.I. Míguez, J.R. Vilche, A.J. Arvía, *Electrochim. Acta,* **32**, 1743 (1987).
30. A. Hugot-Le Goff., J. Flis, N. Boucherit, S. Joiret, J. Wilinski, *J. Electrochem. Soc.* **137**, 2684 (1990).
31. X.R. Novoa, M.C. Perez, C. Rangel, H. Takenouti. *4th International Symposium on Electrochemical Impedance Spectroscopy. Extended abstracts*, p 300. Rio de Janeiro, Brasil, 1998.
32. S. Joiret, M. Keddam, X.R. Novoa, M.C. Pérez, H. Perrot, H. Takenouti. In: *Passivity of Metals and Semiconductors. Proceedings of the 8th International Symposium*, M.B. Ives, J.L. Luo and J. Rodda (Eds.), p.799. The Electrochemical Society, Pennington, NJ, USA, 2001.
33. S. Joiret, M. Keddam, X. R. Novoa, M. C. Pérez, C. Rangel, H. Takenouti, *Cem. Concr. Composites*,. **24**, 7 (2002).
34. B. MacDougall, M.J. Graham, in: *Corrosion Mechanisms in Theory and Practice*, P. Marcus and J. Oudar (Eds.), p.143, Marcel Dekker, N.Y., USA, 1995.

35. D. Landolt, *Corrosion et Chimie des Surfaces des Métaux*, p. 107. Presses Polytechniques et Universitaires Romandes, Laussanne, Switzerland, 1993.
36. C. Alonso, M. Castellote, C. Andrade, *Electrochim. Acta,* **47**, 3469 (2002).
37. C. Alonso, C. Andrade, M. Castellote, P. Castro, *Cem. Conc. Res.* **30**, 1047 (2000).
38. G. Prentice, *Electrochemical Engineering Principles*. p. 102. Prentice-Hall Inc., Englewood Cliffs, N.J., USA, 1991.
39. B.E. Conway. *J. Electrochem. Soc.* **138**, 1530 (1991).
40. C. Andrade, P. Merino, X.R. Nóvoa, M.C. Pérez, L. Soler, *Mater. Sci. Forum,* **192-194**, 891 (1995).
41. B.E. Conway, *Electrochemical Supercapacitors: Scientific Fundamentals and Technological Applications*. Chap. 10. Kluwer Academic/Plenum Pub. N.Y., USA, 1999.
42. C. Andrade, M. Keddam X. R. Nóvoa, M. C. Perez, C. M. Rangel, H. Takenouti. *Electrochim. Acta,* **46**, 3905 (2001).
43. D.G. John, P.C. Searson, J.L. Dawson, *Br. Corros. J.,* **16**, 102 (1981).
44. C. Andrade, L. Soler, X.R. Nóvoa, *Mater. Sci. Forum*, **192-194**, 843 (1995).
45. C. Andrade, L. Soler, C. Alonso, X.R. Nóvoa, M. Keddam, *Corros. Sci.* **37**, 2013 (1995).
46. D.G. John, P.C. Searson, J.L. Dawson, *Br. Corros. J.,*, **16**, 102 (1981).
47. V. Feliu, J.A. González, C. Andrade, S. Feliu, *Corros. Sci.* **40**, 975 (1998).
48. C. Andrade, F. Bolzoni, M. Cabeza, X.R. Nóvoa, M.C. Perez. In: *Electrochemical approach to selected corrosion and corrosion control studies*. Publication No 28 of the European Federation of Corrosion, p. 332, published by The Institute of Materials, London, England, 2000.
49. M. Stratmann, K. Bohnenkamp, H.-J. Engell, *Corros. Sci.* **23**, 969 (1983).
50. N. Sato, G. Okamoto, in: *Comprehensive Treatise of Electrochemistry*, Vol. 4, J. O'M. Bockris, B.E. Conway, E. Yeager, R.E. White (Eds.), p. 214. Plenum Press, N.Y., USA, 1981.
51. C. Alonso, C. Andrade, A. Barreiro, L. Espada, X.R. Nóvoa, *Mater. Sci. Forum*, **289-292**, 45 (1998).

52. C. Alonso, C. Andrade, M. Izquierdo, X.R. Nóvoa, M.C. Pérez, *Corros. Sci.*, **40**, 1379 (1998).
53. C. Alonso, M. Izquierdo, P. Merino, X.R. Nóvoa, *An. Quím.*, **89**, 452 (1993).
54. J.R. Scully, *Corrosion*, **56**, 199 (2000).